Bidirectional Counting of Single Electrons

Toshimasa Fujisawa,[1,2]* Toshiaki Hayashi,[1] Ritsuya Tomita,[1,2] Yoshiro Hirayama[1,3,4]

A bidirectional single-electron counting device is demonstrated. Individual electrons flowing in forward and reverse directions through a double quantum dot are detected with a quantum point contact acting as a charge sensor. A comprehensive statistical analysis in the frequency and time domains and of higher order moments of noise reveals antibunching correlation in single-electron transport through the device itself. The device can also be used to investigate current flow in the attoampere range, which cannot be measured by existing current meters.

Photon counting has been shown to be useful for detecting a faint light and for characterizing nontrivial photon statistics (*1*). Similarly, electron counting is expected to provide a sensitive ammeter and deep insights into correlated transport (*2*, *3*). In contrast to photon counting, in which only incoming photons are considered, electron transport involves the frequent occurrence of backscattering events, which makes bidirectional counting essential for a full understanding of its statistics.

Conventional current noise measurements are successful for characterizing correlated transport (*3*, *4*), such as the sub-Poissonian statistics in single-electron tunneling (*5*) and the fractional quantum Hall effect (*6*, *7*). However, the second-order noise measurements are restricted to strongly nonequilibrium conditions where transport can be considered unidirectional. In addition, these measurements cannot determine correlations of a few electrons, because existing current meters require the movement of millions of electrons. Recently, individual single-electron transport through a quantum dot has been investigated in real time with the use of an integrated charge detector (*8*–*11*), but single-dot charge detection cannot determine the direction of the transport.

We demonstrate a bidirectional single-electron counting (B-SEC) device in which individual electrons tunneling through a double quantum dot (DQD) are detected with a charge sensor made of a quantum point contact (PC). Statistical analysis of forward and reverse tunneling events allows us to determine all parameters that describe the system. We find that two forward tunneling events never occur consecutively; this phenomenon reveals antibunching correlation in the single-electron transport. The third-order noise is insensitive to thermal fluctuations, which allows us to extract the correlation effect even in a nearly equilibrium condition. These statistical methods can also be used to investigate extremely small currents from an external test device.

The operation of our B-SEC device is based on charge detection in a DQD in the Coulomb blockade regime, where higher order tunneling processes can be safely neglected (*12*). The device consists of a DQD (dots L and R) and a PC for charge detection (Fig. 1A). The PC is asymmetrically coupled to the dots (stronger to dot L), so that the current through the PC, I_{PC}, depends differently on the respective electron numbers (n,m) in dots L and R (*13*, *14*). The current through the DQD results in temporal changes in the electron numbers (n,m), which appear as fluctuations in the PC current (Fig. 1B). By observing transitions between (1,0) and (0,1) states, we can regard the current across the central barrier, I_C, as a train of single-electron pulses (Fig. 1C).

A scanning electron micrograph (SEM) of a B-SEC device fabricated in an AlGaAs/GaAs heterostructure is shown in Fig. 1D. The application of appropriate negative voltages on metal gates (gold regions) depletes conductive electrons nearby and forms the integrated device in a desired action (*8*). The PC is adjusted in the tunneling regime, where I_{PC} is sensitive to the charge distribution around the PC. The current, $\langle I_{PC} \rangle \approx 12$ nA on average at an excitation voltage $V_{PC} = 0.8$ mV, changes by a few percent depending on the charge state of the DQD. The charge state (n,m) of the DQD can be controlled by voltages V_L and V_R, respectively, applied to gates G_L and G_R; the average current $\langle I_{PC} \rangle$ shown in Fig. 2A indicates four discrete values depending on (n,m). Clear separation of (0,0) and (1,1) domains indicates an electrostatic coupling energy of ~200 μeV for the DQD (*15*). Similar patterns are observed in a wide range of the V_L-V_R plane, and we select a specific region where all the tunneling rates of the DQD are within the bandwidth (~10 kHz) of the current amplifier used to measure I_{PC}. Then, individual tunneling events can be clearly visible in the time domain, as shown in Fig. 2B. The three-level fluctuation observed at charge triple points E and H (denoting electron-like and hole-like transport, respectively), the two-level fluctuation between (1,0) and (0,1) at M (the middle), and the absence of fluctuation in blockade region B are consistent with expectations.

We record I_{PC} traces over a period $T_p = 1.3$ s with a time resolution of $t_0 = 20$ μs and digitize the current into four values, corresponding to the (n,m) states of interest, with an appropriate filtering and threshold. If required, a group of many (up to 50) traces are used to obtain reliable statistics. All information needed for characterizing the transport can be obtained from the statistics. The residence time $T_{res}^{(n,m)}$, defined as how long the QD stays in a particular charge state (n,m) before changing to another state (as in Fig. 1B), is a stochastic quantity and takes a random value every time (Fig. 2C). The data are taken in the nonlinear conductance regime at a positive bias voltage $V_S = 300$ μV. The exponential distribution is observed for all charge

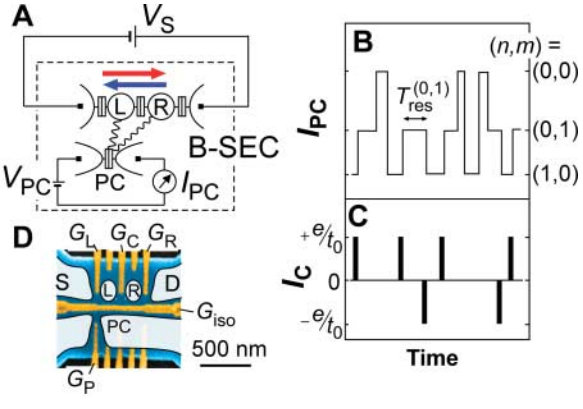

Fig. 1. B-SEC device. (**A**) The B-SEC device consists of a double dot (L and R) and a charge detector (PC). The double boxes represent tunneling barriers; wavy lines illustrate Coulomb interaction and red and blue arrows indicate forward and reverse electron transport, respectively. (**B**) Schematic fluctuation of detector current, I_{PC}, which corresponds to charge state (n,m) with n and m excess electrons, respectively, in dots L and R. (**C**) Pulsed current across the central barrier, I_C. Each current pulse with height e/t_0 and time resolution t_0 of the measurement represent transport of elementary charge e. (**D**) Colored SEM image (blue and black, unetched and etched semiconductor surface, respectively; gold, metal gates; white, conductive regions) of a control device fabricated by standard lithographic techniques. The double dot (L and R) and PC are formed by applying negative voltages to the gates. All measurements were performed at 35 mK at zero magnetic field.

[1]NTT Basic Research Laboratories, NTT Corporation, 3-1 Morinosato-Wakamiya, Atsugi 243-0198, Japan. [2]Tokyo Institute of Technology, 2-12-1 Ookayama, Meguro-ku, Tokyo 152-8551, Japan. [3]Solution Oriented Research for Science and Technology (SORST), Japan Science and Technology Agency, 4-1-8 Honmachi, Kawaguchi 331-0012, Japan. [4]Department of Physics, Tohoku University, Sendai, Miyagi 980-8578, Japan.

*To whom correspondence should be addressed. E-mail: fujisawa@nttbrl.jp

states, indicating a random Poisson process characterized by a single lifetime $\tau_{nm} = \langle T_{res}^{(n,m)} \rangle$ (*8*, *16*), which is related to the sum of all possible tunneling rates $\Gamma_{nm \to ij}$ from (n,m) to (i,j)—that is, $\tau_{nm}^{-1} = \sum_{i,j} \Gamma_{nm \to ij}$. One can also count the number of transition events $N_{nm \to ij}$ from (n,m) to (i,j), which should be proportional to the rates by the relation $N_{nm \to ij} = p_{nm}^0 \Gamma_{nm \to ij} T_p$, where p_{nm}^0 is the occupation probability for (n,m) in a steady condition. By solving these relations, all relevant rates $\Gamma_{nm \to ij}$ and populations p_{nm}^0 can be determined.

Figure 2D shows $N_{nm \to ij}$ obtained from the same data set. The transport is dominated by a cyclic transition (shown by red arrows) from (1,1) through (1,0) to (0,1) and back to (1,1), which carries an electron from the left to the right. Note that non-negligible reverse processes (blue arrows) are also revealed in the present measurements. The very small counting rate [< 30 cps for the transitions involving the (0,0) state] is attributed to noise in the PC current (dark counting) and should thus be disregarded; transitions between (0,0) and (1,1) are unphysical in the sequential tunneling regime. Because of the finite bandwidth, our measurement fails to count very fast successive transitions within 100 μs. These effects are all minor and do not affect our analysis. The obtained rates $\Gamma_{nm \to ij}$ are summarized in Fig. 2E.

We performed similar analyses at various points in the V_L-V_R plane and investigated how the forward and reverse tunneling rates change. We first examined dot-lead tunneling across the left barrier by comparing $\Gamma_{01 \to 11}$ and $\Gamma_{11 \to 01}$. These are plotted in Fig. 2F as a function of the electrochemical potential, $\mu = E_{01} - E_{11}$, where E_{nm} is the total energy of the (n,m) state (*15*). The dependence can be well fitted with solid lines by considering the Fermi distribution in the electrode with an electron temperature of T_e = 130 mK in the lead (*17*). The behaviors of the forward and reverse rates are almost symmetric with respect to $E_{10} = E_{11}$ (dashed line). The small difference (factor of ~1.5) between the maximum saturated rates for the forward and reverse tunneling may be related to spin degeneracy; a factor of 2 difference is expected for transitions between different charge states having total spins of 0 and ½ (*18*). The dot-lead tunneling shows detailed balancing in which the ratio of forward and reverse rates is determined by the electrochemical potential, $\Gamma_{01 \to 11}/\Gamma_{11 \to 01} = \exp[\mu/(kT_e)]$ (where k is the Boltzmann constant), up to degeneracy. In contrast, the interdot tunneling rates $\Gamma_{01 \to 10}$ and $\Gamma_{10 \to 01}$ measure how frequently the system absorbs or emits energy from or to the environment (*19*). As shown in Fig. 2G, the rates deviate from the symmetric dependence in the whole range across some peaks (indicated by arrows) associated with alignments of discrete energy levels in the dots. Violation of detailed balancing implies strong nonequilibrium excitation under back action from the PC detector (*20*).

Although each tunneling process characterized by $\Gamma_{nm \to ij}$ is Poisson random, Coulomb interaction prohibits double occupancy in a small island and correlates the overall electron transport. Charge transport in the sequential tunneling regime can be described by the rate equation $(d/dt)\mathbf{p}(t) = \mathbf{M}\mathbf{p}(t)$, where $\mathbf{p}(t)$ is an array of time-dependent occupation probabilities $\{p_{nm}(t)\}$ (*21*). The matrix $\mathbf{M}$ describes the transition rates consisting of diagonal and off-diagonal terms $-\tau_{nm}^{-1}$ and $\Gamma_{nm \to ij}$, respectively. Because we have already obtained $\mathbf{M}$ as in Fig. 2E, we can calculate the expected average current, noise spectrum (*21*), and higher order moments of noise (*22*), which are more suitable for describing the correlated transport. These statistics can be obtained by analyzing the pulsed current (conserved quantity), which is more versatile even when complete information, such as $\mathbf{M}$, is not available.

We next define three pulsed currents, I_L, I_C, and I_R, which exhibit B-SEC at the left, central, and right barriers, respectively. They are obtained by considering the corresponding tunneling processes as discussed for I_C in Fig. 1C. The average currents obtained for a long period, T_p = 1.3 s, always coincide with each other (i.e., $\langle I_L \rangle = \langle I_C \rangle = \langle I_R \rangle$) as a result of current conservation. The average current $\langle I \rangle$ in the V_L-V_R plane is shown in Fig. 3A. The triangular conductive regions around E and H with a resonant tunneling peak on one side of the triangles are consistent with the energetics for transport through a DQD (*15*).

Noise power spectra S_L, S_C, and S_R (Fig. 3B, top) are obtained from numerical Fourier transforms of the corresponding pulsed currents. The spectra are qualitatively the same as those calculated from $\mathbf{M}$ (Fig. 3B, bottom) (*21*), indicating the validity of our statistical analysis. The enhanced spectrum in the high-frequency part (>1 kHz, the characteristic frequency set by $\mathbf{M}$) is related to how frequently an electron experiences backscattering across the barrier. The low-frequency part, identical for the three spectra, is almost flat except for excess dark-counting noise below 10 Hz. Background charge fluctuation (1/*f* noise), which often dominates low-frequency noise, is suppressed by the digitizing

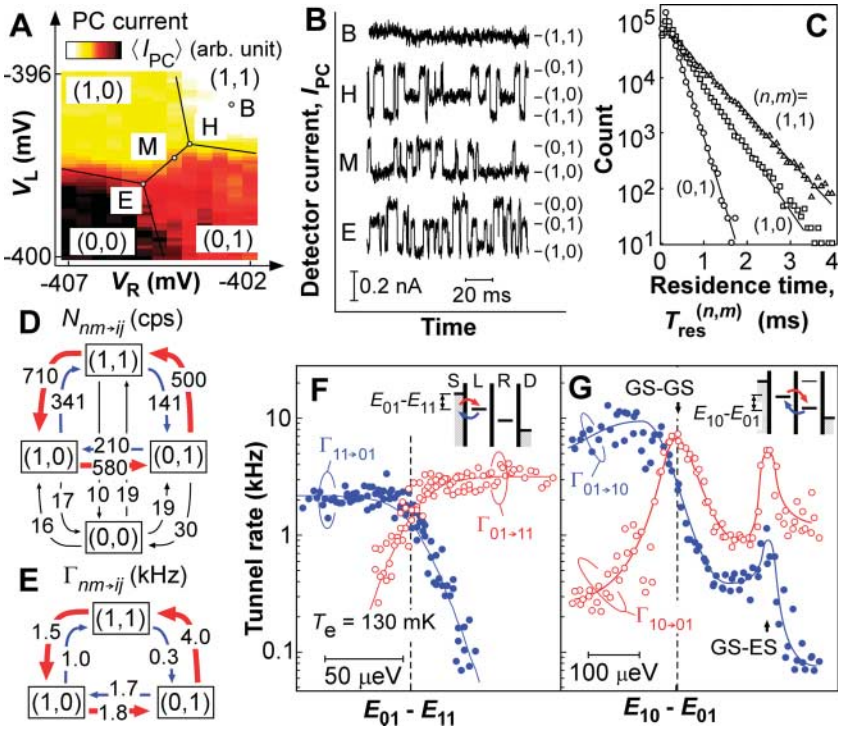

Fig. 2. Statistics of charge fluctuation in a DQD. (**A**) Color plot of the averaged PC current, $\langle I_{PC} \rangle$, in the V_L-V_R plane measured at V_S = 0 and V_{PC} = 0.8 mV, with a stability diagram (n,m) of the DQD. An appropriate linear function of V_L and V_R is subtracted from the raw data to remove electrostatic coupling from the gates. (**B**) Fluctuation of I_{PC} measured at some points shown in (A). Typically, $\langle I_{PC} \rangle \approx 12$ nA. (**C**) Distribution of the residence time T_{res} for (0,1), (1,0), and (1,1) states. (**D**) An example of the number of transition events $N_{nm \to ij}$. (**E**) An example of tunneling rates $\Gamma_{nm \to ij}$. The same data set measured at V_S = 300 μV around point α in Fig. 3A is used for (C), (D), and (E). (**F** and **G**) Forward and reverse rates across left (F) and central (G) barriers. Insets show energy diagrams of the DQD with corresponding tunnel processes. Obtained rates at V_S = 300 μV and various V_L and V_R points are plotted as a function of chemical potential, $E_{01} - E_{11}$ in (F) and $E_{10} - E_{01}$ in (G). Solid lines in (F) are fitted with T_e = 130 mK; solid lines in (G) are guides for the eye. Arrows in (G) represent resonances of the ground state (GS) of one dot to the ground and excited states (ES) of the other dot.

process. The noise level in the 10 to 100 Hz range is suppressed below full shot noise $2e\langle I\rangle$ (dashed line), indicating correlated transport (*5*). In fact, we find that B-SEC provides better statistics that identify the antibunching correlation directly. The distribution of the time interval, t_{++}, between two successive forward current pulses (Fig. 3C) is no longer a simple exponential, and suppression of consecutive forward pulses at $t_{++} \approx 0$ (antibunching) is directly identified, consistent with a rate-equation calculation (solid curve). Note that the broad peak in the distribution indicates quasi-periodic current as a precursor of single-electron tunneling oscillations (*10*).

We can extract other statistics often used in quantum optics, such as electron (photon) number distribution (*1*, *2*, *23*). The third-order moment of the distribution, which is called skewness, is of particular interest for its insensitivity to thermal distribution (*24*–*26*) and is considered to be a new tool for investigating correlated transport, valid even for near-equilibrium conditions. Gustavsson *et al.* used charge detection measurement on a single quantum dot to identify correlated transport from its second- and third-order noise (*11*). Taking advantage of bidirectional counting in our device, we have shown that the third-order noise is insensitive to the thermal noise (supporting online text).

The reverse problem of identifying unknown correlation would be useful in many cases. The top part of Fig. 4A illustrates a circuit for counting electrons from a test device. Although it is impossible to obtain all information about the test device, one can obtain useful information by means of time, frequency, and momentum analyses with a B-SEC device. For this purpose, the impedance of the B-SEC device should be smaller and its correlation time shorter than that of the test device (*27*). Our B-SEC device can be applied to investigate extremely small current from a high-impedance test device, and this is precisely what conventional electronics cannot cover. In Fig. 4A we show how our device performs as a current meter, using another single quantum dot as a test device. The average current $\langle I\rangle$ obtained from the B-SEC device reasonably depends on two gate voltages, V_A and V_B, of the test device (Fig. 4B), indicating that the observed Coulomb blockade peaks are associated with the test device. The peak-to-peak noise level in the blockade region is 3 aA for an averaging time of 1.3 s, which is about three orders of magnitude smaller than that in conventional current meters.

The demonstrated B-SEC device enables the use of various statistical analyses to characterize the correlation, and it is also useful for investigating extremely small currents. Integration with other mesoscopic electron devices, such as beam splitters or interferometers, would lead to various techniques for exploring nontrivial intensity correlation and entanglement in mesoscopic electron systems (*28*).

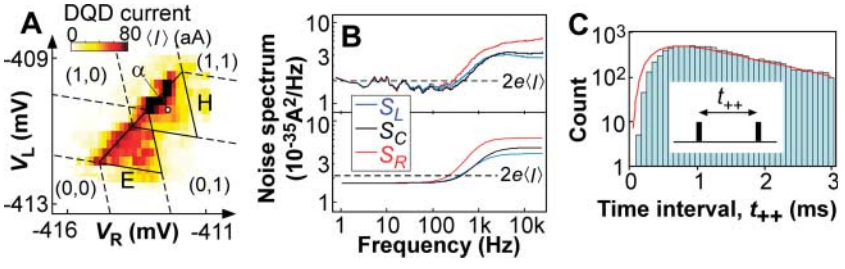

Fig. 3. Statistics of current at the left, central, and right barriers. (**A**) Average current $\langle I\rangle$ in the V_L-V_R plane at V_S = 300 μV. Triangles E and H define conductive regions. (**B**) Noise power spectra, S_L, S_C, and S_R, of the corresponding currents. The upper panel shows the power spectrum of the pulsed current; the lower panel shows the spectrum of the correlation function derived by solving rate equations. The dashed line denotes full shot noise $2e\langle I\rangle$. (**C**) Distribution of the time interval between successive forward tunneling events in I_C. The solid curve shows calculated occurrence of the conditional event derived from the corresponding rate equations. The inset illustrates the time interval, t_{++}. The data set used for (B) and (C), as well as for Fig. 2, C to E, was taken in the nonlinear conductance regime [point α in (A)].

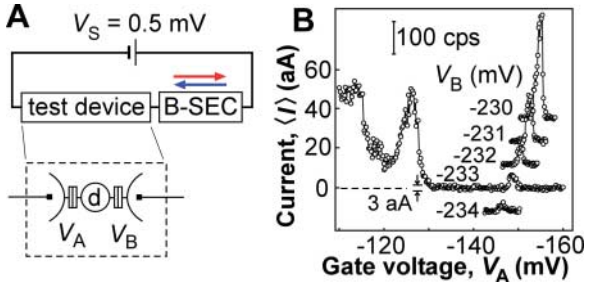

Fig. 4. Single-electron counting for an external test device. (**A**) Measurement diagram with a QD (d) test device fabricated with the same technique as the B-SEC device. Tunneling rates of the two barriers on both sides of the QD can be controlled with voltages V_A and V_B. The net electron flow rate (current) is obtained by subtracting the reverse counting rate (blue arrow) from the forward rate (red arrow). (**B**) Average current obtained from the B-SEC device. Current ranging from −10 to 50 aA can be measured with a voltage drop of ~200 μV across the present B-SEC device. The observed Coulomb blockade peak changes with V_B. Each trace is offset for clarity.

References and Notes

1. R. Loudon, *The Quantum Theory of Light* (Oxford, New York, 1973).
2. L. S. Levitov, H. Lee, G. B. Lesovik, *J. Math. Phys.* **37**, 4845 (1996).
3. Yu. V. Nazarov, Ed., *Quantum Noise in Mesoscopic Physics*, Vol. 97 of *NATO Science Series II* (Kluwer, Dordrecht, Netherlands, 2003).
4. Ya. M. Blanter, M. Büttiker, *Phys. Rep.* **336**, 1 (2000).
5. H. Birk, M. J. M. de Jong, C. Schönenberger, *Phys. Rev. Lett.* **75**, 1610 (1995).
6. L. Saminadayar, D. C. Glattli, Y. Jin, B. Etienne, *Phys. Rev. Lett.* **79**, 2526 (1997).
7. R. de Picciotto *et al.*, *Nature* **389**, 162 (1997).
8. T. Fujisawa, T. Hayashi, Y. Hirayama, H. D. Cheong, Y. H. Jeong, *Appl. Phys. Lett.* **84**, 2343 (2004).
9. W. Lu, Z. Ji, L. Pfeiffer, K. W. West, A. J. Rimberg, *Nature* **423**, 422 (2003).
10. J. Bylander, T. Duty, P. Delsing, *Nature* **434**, 361 (2005).
11. S. Gustavsson *et al.*, *Phys. Rev. Lett.* **96**, 076605 (2006).
12. H. Grabert, M. H. Devoret, Eds., *Single Charge Tunneling: Coulomb Blockade Phenomena in Nanostuctures* (Plenum, New York, 1991), chap. 3.
13. M. Field *et al.*, *Phys. Rev. Lett.* **70**, 1311 (1993).
14. J. R. Petta *et al.*, *Science* **309**, 2180 (2005); published online 1 September 2005 (10.1126/science.1116955).
15. W. G. van der Wiel *et al.*, *Rev. Mod. Phys.* **75**, 1 (2003).
16. N. G. van Kampen, *Stochastic Processes in Physics and Chemistry* (Elsevier, Amsterdam, 1992).
17. D. H. Cobden, B. A. Muzykantskiĭ, *Phys. Rev. Lett.* **75**, 4274 (1995).
18. D. H. Cobden, M. Bockrath, P. L. McEuen, A. G. Rinzler, R. E. Smalley, *Phys. Rev. Lett.* **81**, 681 (1998).
19. T. Fujisawa *et al.*, *Science* **282**, 932 (1998).
20. R. Aguado, L. P. Kouwenhoven, *Phys. Rev. Lett.* **84**, 1986 (2000).
21. S. Hershfield, J. H. Davies, P. Hyldgaard, C. J. Stanton, J. W. Wilkins, *Phys. Rev. B* **47**, 1967 (1993).
22. D. A. Bagrets, Yu. V. Nazarov, *Phys. Rev. B* **67**, 085316 (2003).
23. M. Ueda, *Phys. Rev. A* **40**, 1096 (1989).
24. L. S. Levitov, M. Reznikov, *Phys. Rev. B* **70**, 115305 (2004).
25. B. Reulet, J. Senzier, D. E. Prober, *Phys. Rev. Lett.* **91**, 196601 (2003).
26. Yu. Bomze, G. Gershon, D. Shovkun, L. S. Levitov, M. Reznikov, *Phys. Rev. Lett.* **95**, 176601 (2005).
27. C. W. J. Beenakker, M. Kindermann, Yu. V. Nazarov, *Phys. Rev. Lett.* **90**, 176802 (2003).
28. P. Samuelsson, E. V. Sukhorukov, M. Büttiker, *Phys. Rev. Lett.* **92**, 026805 (2004).

29. We thank L. S. Levitov, K. Muraki, Yu. V. Nazarov, Y. Tokura, M. Ueda, and Y. Yamamoto for valuable comments. Supported by the Strategic Information and Communications R&D Promotion Program (SCOPE) from the Ministry of Internal Affairs and Communications of Japan, and by a grant-in-aid for scientific research from the Japan Society for the Promotion of Science.

Supporting Online Material

www.sciencemag.org/cgi/content/full/312/5780/1634/DC1
SOM Text
Figs. S1 and S2
References

28 February 2006; accepted 27 April 2006
10.1126/science.1126788